

**Understanding Paclitaxel / Pluronic F127 Nanocrystals Prepared by the
Stabilization of Nanocrystal (SNC) Method**

Jiexin Deng

A thesis submitted to the faculty of the University of North Carolina at Chapel Hill in partial fulfillment of the requirements for the degree of Master of Science in the Division of Molecular Pharmaceutics at Eshelman School of Pharmacy.

Chapel Hill
2009

Approved by

Philip Smith, Ph.D.

Feng Liu, Ph.D.

Moo J Cho, Ph.D.

©2009
Jiexin Deng
ALL RIGHTS RESERVED

Abstract

Jiexin Deng : Understanding Paclitaxel / Pluronic F127 Nanocrystals Prepared by the Stabilization of Nanocrystal (SNC) Method

(Under the direction of Dr. Feng Liu and Dr. Leaf Huang)

The objectives of this study were to understand the structure and stability of paclitaxel nanocrystals, as well as the biodistribution of nanocrystals after intravenous injection in mice. The nanocrystal size increased after 2 h 37 °C incubation due to thermal induced aggregation. The addition of more F127 surfactant further destabilized nanocrystals and led to a larger size increase concurrent with micelle formation. PTX/F127 nanocrystals (1/5 w/w) had little size increase upon dilution, indicating tight monomer surfactant absorption. Nanocrystals of more F127 surfactant (1/20, 1/30 w/w) increased much in size upon dilution, suggesting low-affinity surfactant absorption with micelle formation in solution. The re-nanonization after 37 °C incubation effectively inhibited crystal growth after 37 °C incubation again by disturbing the preferred crystal growth pattern of PTX. The biodistribution of nanocrystals revealed that the majority of nanocrystals were quickly taken up by reticuloendothelial system and went to the liver 1 h post injection.

Acknowledgements

First of all, I would like to thank Dr. Leaf Huang, my research advisor. I have the fortune of knowing Dr. Huang as a research advisor, teacher, and also as a preacher at my church. I have to say that Dr. Huang is a good teacher as well as an excellent preacher, and I have learned much from him in both roles. Dr. Huang has challenged me to show my best efforts as a graduate student, as well as provided much advice to me about life. I would also like to thank Dr. Feng Liu for mentoring me in the lab. Dr. Feng Liu has shaped the way I approach science and taught me to be a good experimenter that put my heart into everything that I do. Dr. Feng Liu just has been such an integral part of my graduate student life, and I could not thank him more for his excellent mentoring. I would like to thank my two other committee members, Dr. Moo J Cho and Dr. Philip Smith. I have to thank them for facilitating this project and providing excellent expertise. I would like to thank all members of the Huang Lab for providing help, support, and friendship. Also, thanks goes to the administrative staff, Angela Lyght, Kathryn Fiscelli, Kim Hoenerhoff, and Amber Allen for taking care of miscellaneous matters. Finally, I would like to thank my parents, Dr. Jinbo Deng and Ping Wu, as well as my little brothers, Delai Deng and Weibo Deng, for providing me the best family love and support.

Table of Contents

LIST OF TABLES	vi
LIST OF FIGURES	vii
ABBREVIATIONS	vii
INTRODUCTION	1
MATERIALS AND METHODS	4
RESULTS	9
DISCUSSION	19
CONCLUSION	26
REFERENCES	50

LIST OF TABLES

Table 1: X-Ray Powder Diffraction Peaks	27
Table 2: Nanocrystal size after 2 h 37 °C incubation	28
Table 3: Manually measured nanocrystal size after 2 h 37 °C incubation	29
Table 4: Manually measured nanocrystal size after re-nanonization	30
Table 5: XRD of re-nanonized nanocrystals	31
Table 6: HPLC extraction difference between Taxol [®] and nanocrystals	32

LIST OF FIGURES

Figure 1: X-Ray Powder Diffraction Peaks	33
Figure 2: PTX crystals Alone without F127 and PTX/F127 Physical Mixture	34
Figure 3: TEM pictures of nanocrystals for thermal stability studies	35
Figure 4: Effects of increasing F127 on nanocrystal cytotoxicity	36
Figure 5: TEM of nanocrystals of 1/10 and 1/20 w/w PTX/F127	37
Figure 6: Illustration of nanocrystals stabilized by F127	38
Figure 7: Nanocrystal size increase upon dilution at room temperature	39
Figure 8: TEM of undiluted sample at the end of dilution-size experiment	41
Figure 9: Illustration of size increase of nanocrystals upon dilution	42
Figure 10: Nanocrystal (1/5 w/w PTX/F127) size increase upon dilution at 37 °C	43
Figure 11: Re-nanonization by Incubation-Sonication procedure	44
Figure 12: Nanocrystal TEM pictures after Incubation-Sonication procedure	45
Figure 13: Cytotoxicity of nanocrystals after Incubation Sonication procedure	46
Figure 14: Extraction procedure of PTX with addition of acetonitrile	47
Figure 15: Plasma and organs PTX extraction standard curves	48
Figure 16: Nanocrystal biodistribution in mice plasma and organs	49

Abbreviations

F127:	diblock copolymer Pluronic F127
H460:	NCI-H460 human lung cancer cells
MTT:	3-(4,5-Dimethylthiazol-2-yl)-2,5-diphenyltetrazolium bromide
PTX:	paclitaxel
RES:	reticuloendothelial system
SNC:	stabilization of nanocrystals
TBME:	tert-butyl methyl ether
TEM:	transmission electron microscope
XRD:	X-ray powder diffraction

Introduction

Paclitaxel (PTX), the first of a new class of microtubule stabilizing agents, has demonstrated significant antitumor activity in clinical trials against a broad range of solid tumors, including refractory ovarian cancer, metastatic breast cancer, non-small-cell lung cancer, AIDS-related Kaposi's sarcoma^{1,2}. PTX is a highly hydrophobic diterpenoid pseudoalkaloid (of 853 Da³) with poor aqueous solubility of approximately 1 µg/mL⁴. It is currently formulated as Taxol, a concentrated solution containing 6 mg PTX/mL of Cremophor EL (polyoxyl 35 castor oil) and dehydrated alcohol (1:1, v/v)². However, Cremophor EL component of the drug formulation is thought to be responsible for hypersensitivity reactions approaching some 25 to 30 percent of patients, since it can induce histamine release by mast and basophil cells⁵. Therefore, novel formulations of paclitaxel alternative to the commercial ones are still highly desirable.

Attempts to solubilize poorly water soluble drugs such as paclitaxel using co-solvents, in micelles, in liposomes, or with cyclodextrin has been of limited success. An alternative formulation is nanosuspensions which are sub-micron colloidal dispersions of pure particles of drug that are stabilized by surfactants⁶. Contrary to conventional approach of solubilizing insoluble drugs with excess amounts of co-solvents, nanosuspensions forgo the need of solubilization by stabilizing nano-sized drug crystals acceptable for pharmaceutical uses. According to Noyes-Whitney and Ostwald-Freundlich principles, homogeneous particle sizes of nanosuspension in nanometer range

can lead to increased dissolution velocity and saturation solubility, thus increase in bioavailability^{7,8}. Nanosuspensions could be given in various routes of administrations such as oral⁹, parenteral¹⁰, ocular¹¹, and pulmonary delivery¹². These nanosuspension studies by different routes of administration have revealed benefits such as increased rate and extent of absorption, increased bioavailability, reduced administration volumes, and increased resistance to hydrolysis and oxidation¹³. Pharmacokinetic profiles of intravenous administration have shown the sustained release of nanosuspension by slowing diffusing out of monocyte phagocytic system following uptake for prolonged periods of time¹³.

One such nanosuspension formulation is PTX nanocrystals prepared using simple method of stabilization of nanocrystals (SNC) using a diblock copolymer Pluronic F127 as the sole excipient¹⁴. PTX is relatively complex organic drug having several solid structures such as crystal and amorphous, and the stabilized amorphous aggregate of PTX and F127 co-precipitation played an important role in SNC method. The amorphous co-precipitate provided the flexibility such that minimal energy and F127 were required in the nanoparticle forming process, and this resulted in simple preparation and high drug loading efficiency¹⁴. The resulting nanoparticle formulation has low toxicity due to low PTX to F127 ratio, and the nanoparticle can bring higher amount of drug to cancer cells upon delivery. In this study we would like to further understand the structure and stability of PTX/F127 nanocrystals, as well as the biodistribution of the nanocrystals after IV injection in mice. X-ray powder diffractions were performed to evaluate the crystalline state of the nanocrystal samples. The effects of increasing concentration of F127 surfactant on nanocrystal stability after 2 h 37 °C incubation were studied using

light scattering ZetaSizer. TEM pictures of nanocrystal samples were taken to observe the morphology, crystal growth, and micelle formation in our samples. F127 surfactant desorption from nanocrystals, and subsequent size increase, due to water dilution was studied with increasing surfactant concentration at room temperature and 37 °C. The “Incubation-Sonication” procedure was used to make stable nanocrystals that resisted growth during 37 °C incubation. Finally, the biodistribution of nanocrystals in mice plasma and organs 1 h post injection was evaluated.

Materials and Methods

Animals and Materials. Female BALB/c mice (5 weeks old) were purchased from National Cancer Institute U.S. National Institute of Health (NCI). Human lung cancer cell line, NCI-H460, was obtained from American Type Culture Collection. All work performed on animals was in accordance with and permitted by the University of North Carolina Institutional Animal Care and Use Committee. Paclitaxel (PTX) was bought from Lc Laboratories (Woburn, MA). Pluronic F-127 (F127), Cremophor-EL, Butyl-4-hydroxybenzoate, and tert-butyl methyl ether (T-BME) were purchased from Sigma.

Preparation of the PTX samples. The nanocrystals were prepared by the method of stabilization of nanocrystals (SNC). Briefly, paclitaxel (PTX) and F127 were first dissolved in chloroform (in a glass tube) with a weight ratio of 1/5, 1/10, 1/20, or 1/30 (PTX/F127) and then co-precipitated by evaporating the chloroform with a steady stream of nitrogen gas. Traces of chloroform were then removed by keeping the samples under a vacuum with desiccators for 30 min. Following 30 min of hydration (in double deionized water) and vortex, suspensions of the crystal were sonicated for 5 min by a bath-type sonicator (output 80 kc, 80 Watts) to form nanocrystals. After hydration for 20 min, the samples were sonicated for another 5 min. For the physical mixture of PTX/F127, PTX and F127 were not co-dissolved in chloroform and were not co-

precipitated by evaporating the chloroform. Only PTX was dissolved in chloroform, and the chloroform was evaporated with a stream of nitrogen, leaving PTX residues at the bottom of the tube. Then aqueous F127 solutions of appropriate concentration were added to the residues of PTX to make the final weight ratio of 1/5 PTX/F127 w/w. The mixture was then hydrated and sonicated in the same way as described for nanocrystals.

Transmission Electron Microscope (TEM). Transmission electron microscopy (TEM) images of the resulting nanocrystals were acquired using a Phillips CM12 (FEI, Hillsboro, OR). Freshly prepared nanoparticle samples (5 μ l) were dropped onto a 300 mesh carbon-coated copper grid (Ted Pella, Inc., Redding, CA) and allowed a short incubation (5 min) at room temperature. Grids were then stained with 1% uranyl acetate (40 μ l) and wicked dry. All images were acquired at an accelerating voltage of 100 kV. Gatan DigitalMicrograph software was used to analyze the images.

Nanocrystal Size. The distribution of cumulative particle size in the nanocrystal formulation was measured using ZetaSizer Nano-ZS of Malvern Instrument (Westborough, MA). To study the effects of dilution on nanocrystal size, 1 ml of undiluted sample (143 μ g PTX/mL H₂O), 10 fold diluted sample, 50 fold diluted sample were placed in particle size measurement cuvette. These samples were left standing at room temperature or incubated in 37 °C, and at various time points their particle size were measured.

X-Ray Powder Diffraction. The X-ray powder diffraction (XRPD) patterns for Paclitaxel samples were obtained with a Rigaku Multiflex diffractometer. The X-ray source was Ni filtered CuK-alpha radiation (Wavelength 1.5418 Å). The X-ray tube was run at a power of 40 kV, 40 mA. The sample size was approximately 60 mg. The 2θ range scanned was 7.5 to 60° at a rate of 0.25 deg 2θ/min at increments of 0.02° 2θ.

H460 Cell Cytotoxicity Study. The cytotoxicity of nanocrystals on NCI-H460 human lung cancer cells were determined by MTT assay. Briefly, H460 cells were seeded into 96-well plates at a concentration of 1×10^4 cells/well in a volume of 200 µl per well. After 24 h, 20 µl of phosphate buffered saline (PBS) containing the nanocrystals were applied to H460 cells to make the final concentration to be 100 nM of PTX. After 43 hour of incubation, 20 µl of MTT (3-(4,5-Dimethylthiazol-2-yl)-2,5-diphenyltetrazolium bromide) solution (3.33 mg/ml) was added to cell medium in each well. Following 2 hour of incubation with MTT, medium were removed and 100 µl of dimethyl sulfoxide (DMSO) was added to dissolve the formazan crystals. The absorbance values were then measured on a microplate reader (Hidex Plate Chameleon, Turku, Finland) at the wavelength of 570 nm. Cell viability was calculated using the following formula: %viability = (A_{570 nm} for the treated cells / A_{570 nm} for the control cells) × 100%, where A_{570 nm} is the absorbance.

Biodistribution of Paclitaxel Formulations. Biodistribution study of paclitaxel was performed on Balb/C mice, and the animals were kept in the animal facility and had

free access to food and water. For administration, nanocrystal (1/5 w/w PTX/F127) formulations were suspended in certain volumes of PBS (pH 7.4) in order to obtain the required concentration. The different formulations were injected through the tail vein at the paclitaxel dose of 20 mg/kg mouse, and each group consisted of 5 animals. One hour after injection, blood and organs (liver, lung, spleen, kidney) were collected. Blood was obtained from the retro orbital plexus, and plasma was obtained by immediately centrifuging blood samples with EDTA at 7000 g for 5 min. Harvested tissues were stored at -20 °C until analyzed for paclitaxel by HPLC.

HPLC Analysis of Paclitaxel. HPLC method was used for the analysis of paclitaxel concentration in all samples. For plasma samples, 200 µL of plasma was spiked with 10 µL of butyl-4-hydroxybenzoate (50 µg/mL) as internal standard. For paclitaxel plasma standard curve 20 µL of paclitaxel of appropriate concentrations along with the internal standards were dissolved in the plasma samples. After addition of 100 µL of acetonitrile, the plasma samples were then extracted with 2 mL of tert-butyl methyl ether (T-BME) with vigorous mixing for 5 minutes. After centrifugation at 3000 rpm for 5 minutes, the organic phase was collected. The extraction procedure was repeated with 2 mL of T-BME, and total organic phase was combined and dried under nitrogen gas. The residue was then dissolved in 100 µL of the mobile phase, 45% acetonitrile / water. The solution was centrifuged for 5 min at 3000 rpm, and 50 µL of the supernatant was injected into the HPLC system for analysis.

For tissue organs, the tissue samples (liver, spleen, lung, kidney) were homogenized with 1 mL of water Bovine Serum Albumin (BSA) solution, containing 4%

(w/v) bovine serum albumin, using a tissue homogenizer for 5 min at 4 °C. The tissue homogenate (1.0 mL) was spiked with 10 µL of internal standard (Butyl-4-hydroxybenzoate, 50 µg/mL). For paclitaxel organs standard curve 20 µL of paclitaxel of appropriate concentrations along with the internal standards were dissolved in the organ samples. The samples were then extracted twice with 2 mL of T-BME as described for the plasma sample. The T-BME fractions were then combined and were dried under nitrogen gas. The residue was dissolved with 100 µL of mobile phase, 45% Acetonitrile / Water, and was mixed for 5 minutes. The solution was centrifuged at 3000 rpm for 5 min, and 10 µL of the supernatant was injected into the HPLC system for analysis. The HPLC system was performed at a flow rate of 1.0 ml/min at 228 nm with a UV detector, using a 25mm × 4.6 I.D. mm reverse phase Analytical column of Axxiom Chromatography (Moorpark, CA).

Statistical Analysis. All statistical analyses were performed by a two-tailed student *t*-test. Data were considered statistically significant when the *P* value was less than 0.05.

Results

A. Understanding the Structure and Stability of PTX / F127 Nanocrystals

1. Crystalline Structure Identification of Nanocrystals

Although nanocrystals could be observed under TEM, the crystalline structure of nanocrystals was never evaluated. Therefore X-ray powder diffraction analysis was carried out for nanocrystals (PTX/F127 1/5 w/w) as well as physical mixture in comparison with pure PTX and F127. Figure 1 shows the X-ray diffraction peaks for pure paclitaxel, pure F127, nanocrystals, and PTX/F127 physical mixture. As shown in figure 1, the X-ray diffraction pattern of the nanocrystals showed the combined peaks of both of the pure components (paclitaxel and F127). The F127 peaks were much more prominent than the peaks of paclitaxel near the base line at 2θ of 10° to 15° , this is because F127 were present in larger weight ratio (1/5) in the formulation. The X-ray powder diffraction confirmed that in nanocrystal formulation both Paclitaxel and F127 components retained their native crystalline structure. X-ray diffraction peaks for physical mixture were also shown in figure 1c. The diffraction peaks for nanocrystal and PTX/F127 physical mixture were highly similar. Table 1 is a summary of the major X-ray diffraction peaks for each sample, and the nanocrystals and physical mixture had peak characteristics of PTX and F127.

From x-ray diffraction pattern, nanocrystals and the PTX/F127 physical mixture were highly similar in composition and crystalline structure. However, as could be expected the crystal formation in nanocrystal samples and the physical mixture were very different. As shown in figure 2b, the crystal growth of PTX alone with out surfactant was vastly different than that of nanocrystal in shape and pattern. Nanocrystals were rod-shaped structures stabilized by F127 surfactant on the surface; on the other hand, PTX alone formed small trunks of irregular crystals and aggregated with each other. Figure 2c shows the aggregate formed in PTX/F127 physical mixture. While there were resemblances of rod-shaped crystals, these individual crystals collapsed and aggregated with each other forming a mass. Due to the lack of the co-solvation (in chloroform) and co-precipitation step, F127 surfactant in physical mixture could not be adequately coated on the surface of nanocrystals to prevent the aggregation.

2. Effects of Increasing Surfactant on Thermal Stability of Nanocrystals

It is known that the aggregation efficiency of hydrophobic particles would be enhanced at higher temperatures¹⁵. As shown in figure 3 this is also true for our nanocrystals, and after 37 °C incubation for 2 hours longer crystals were formed despite the fact that nanocrystals were stabilized by F127 surfactant. The size as measured by the ZetaSizer went from 176 nm to 258 nm after 2 hour incubation at 37 °C. Therefore, to attempt to further protect the nanocrystals, higher amounts of F127 surfactant were used to prepare PTX/F127 nanocrystals of ratios 1/10, 1/20, and 1/30 w/w. On the contrary, as shown in Table 2 the measured size after 37 °C incubation increases with higher amount

of F127 surfactant used. The measured size for PTX/F127 (1/5 w/w) after 37 °C incubation was 258 nm, but for PTX/F127 (1/20 w/w) and (1/30 w/w) the sizes were 359 and 441 nm respectively after 37 °C incubation.

Due to the inaccuracies of measurement by ZetaSizer for rod-shaped crystals, manual measurements were performed for the TEM pictures, and the results were shown in Table 3. At least 20 crystals of various field-views were measured for each sample, and the average values with standard deviations were given. For nanocrystals prepared with 1/5 w/w of F127, the sizes both before and after 37 °C were statistically smaller than the sizes of crystals with higher concentration of F127. The manual measuring in TEM confirmed the trend in size change measured by the ZetaSizer. Adding more F127 surfactant to the preparation did not help to increase the stability of nanocrystals during 2 h 37 °C incubation.

In order to observe the effects of increasing concentrations of F127 on the cytotoxicity of nanocrystals, PTX nanocrystals with different concentrations of F127 surfactants (1/10, 1/20, 1/30 w/w) were prepared and were applied to NCI-H460 cells. As shown in figure 4, F127 alone at all concentrations (1/10, 1/20, 1/30 w/w) did not cause significant cytotoxicity. Also, the increase in F127 concentrations in nanocrystal formulations did not have significant effects on cell viability, as the nanocrystals treatment groups all had about 45% cell viability regardless of the concentration of F127. Therefore increasing F127 concentrations did not alter the cytotoxic effects of nanocrystals on NCI-H460 cells.

The reason why increasing amount of F127 did not help to further stabilize nanocrystals during 2 h 37 °C incubation became clear in figure 5, which showed that the

formation of micelles was evident at higher concentration of F127 surfactant. The CMC of Pluronic F127 at 25 °C is $7.19 \times 10^{-5} \text{ M}^{27}$. The concentration of F127 in nanocrystals prepared with 1/5 w/w of PTX/F127 is below the CMC of F127. However, for 1/10, 1/20, and 1/30 of PTX/F127, the concentration of surfactant goes beyond the CMC. Instead of forming a thicker coating layer, the additional F127 formed micelles that competed for nanocrystal surface adsorption. Unimers of F127 surfactant bound the surface of nanocrystals with high affinity due to hydrophobic interactions. As the concentration of F127 increased however, surface monomers interacted with each other, forming “hemimicelles” on the surface of nanocrystals that bound with lower affinity than monomers. These lower affinity surfactant could easily be competed off the nanocrystal surface. So this could actually mean less surface adsorption due to competition by micelles as more F127 surfactant was added to the sample, and less surface adsorption means less stability for nanocrystals during 2 h 37 °C incubation.

3. The Effects of Dilution on Surfactant Adsorption and Nanocrystal Stability

Upon IV injection nanocrystals would be diluted many folds in the blood stream, therefore, it would be important to understand the effects of water dilution on surfactant adsorption and nanocrystal stability. As shown in Figure 6, our nanocrystals are in a meta-stable state stabilized by surface adsorbed F127 surfactant. At low concentration of F127 (1/5 w/w PTX/F127) monomers bind with high affinity. At high concentration of F127, monomers aggregated and bind to surface with low affinity; there is also micelle formation competing for surface adsorption. In this experiment, nanocrystal samples

were diluted 10 fold or 50 fold to attempt to draw the adsorbed surfactant layer into free form. By doing so, it is expected that the particle size of PTX nanocrystals would increase upon dilution if surfactant does indeed leave. ZetaSizer measures the size of particles using light scattering from only one angle rather than multiple angles, and there would be measurement inaccuracies for our long rod-shaped PTX crystals. However, the ZetaSizer does give a cumulative measurement of total particle size in solution and is more than capable of giving an idea of the level of crystal aggregation.

As seen in figure 7a, PTX nanocrystals prepared with 1:5 w/w of F127 increased a little in size as time went on however, size increase upon dilution was not observed. As shown by 7b to 7d, the crystal size of nanocrystals formulations containing higher amounts of F127 (1/20, 1/30 w/w) drastically increased upon dilution. In TEM pictures of figure 8, micelle formations were evident in undiluted samples with higher F127 concentration at the end of the dilution-size experiment. These data indicate that the affinity of surfactant binding to the surface of nanocrystals at low concentration of surfactant (1/5 w/w) was not the same as that of nanocrystals with high concentration of surfactant (1/20, 1/30 w/w). At low concentration of F127 (1/5 w/w), no micelles were observed in TEM, and it is likely that monomers bound to nanocrystals with high affinity, and dilution could not pull the surfactant off the surface. At higher concentration of F127 (1/20, 1/30 w/w), micelles started to form that would compete for surface adsorption of F127 (Figure 9). Also, the size increase upon dilution of the nanocrystals of 1/20 and 1/30 PTX/F127 suggests that the surfactant bound with lower affinity, coming off easily upon dilution. It is likely that as F127 concentration increased, monomers started to lose

the high affinity to surface of nanocrystals and would instead interact more with each other.

The Critical Micelle Concentration (CMC) of F127 would decrease drastically from 0.3 wt % at room temperature to 0.025 wt % at 37 °C¹⁶. Therefore, it would be interesting to find out whether the nanocrystal size increases upon dilution at 37 °C where micelle formation would be enhanced. As shown in figure 10, for PTX/F127 1:5 w/w the nanocrystal size indeed increased upon dilution at 37 °C. This suggests that monomers on the surface of nanocrystals started to aggregate at higher temperature and was drawn to leave the crystal surface upon dilution, making the crystal prone to aggregate. This size increase upon dilution for nanocrystals of 1/5 w/w PTX/F127 was not observed at room temperature, where no micelles were formed.

4. Increase of Nanocrystal Stability by Re-nanonization

The crystal growth of nanocrystals after 37 °C incubation presents storage problems, because long crystals could also form at room temperature after preparation or reconstitution due to Ostwald ripening^{17,18}. To solve this problem, sonication for 15 minutes was used to break down the longer crystals after incubation at 37 °C, resulting in smaller nanocrystals again, and the sonicated nanocrystals were then incubated at 37 °C for 2 hours again to see if the incubation would cause regrowth into longer crystals (Figure 11). As shown by Figure 12, the “incubation-sonication” procedure effectively prevented the growth of nanocrystals at 37 °C incubation and provided a much better thermal stability for nanocrystals. It is assumed that the crystal growth pattern would be

disturbed by sonicating large nanocrystals after 37 °C incubation, and it would be difficult to regrow crystals into longer needle-like crystals, thus providing better stability.

To confirm, manual measurements were performed in TEM pictures, and the results with standard deviations were given in Table 4. According to the measurements, the second time 37 °C incubation did not induce statistically significant increase in length after the “incubation-sonication” procedure. Rather the increase in width in sample C was significant. This showed that the “incubation-sonication” procedure made it difficult for crystals to regrow in length, which is the preferred growth pattern for PTX crystals. Thus, this procedure provided overall inhibition of crystal growth and better crystal stability.

The cytotoxic effects of nanocrystal on NCI-H460 cells after the “Sonication-Incubation” procedure were studied. As shown in figure 13, the different treatments of 10 μM PTX were 1) before 2 hr 37 °C incubation, 2) after 2 hr 37 °C incubation, 3) after 2 hr 37 °C incubation then sonication, 4) after 2 hr 37 °C incubation then sonication then 2 hr 37 °C incubation again. The different preparative procedures did not cause significant differences in cytotoxicity, and the cell viability were 40 to 45% across all treatment groups. The crystalline state of nanocrystals after “Sonication-Incubation” procedure were also evaluated using X-ray Powder Diffraction analysis. It was found that the nanocrystal crystallinity was unaltered by procedures such as 37 °C incubation and sonication (Table 5).

B. Biodistribution of Nanocrystals

1. The Difference in Extraction Efficiency of Taxol[®] and Nanocrystal

PTX samples were extracted from plasma and tissue samples and were subsequently analyzed by HPLC in the biodistribution study. To investigate whether there was extraction efficiency differences between the two PTX formulations, 600 μL of blood was spiked with 50 μg of paclitaxel formulations (Taxol[®] and nanocrystals), then the blood was centrifuged at 7000 g for 5 minutes to separate the plasma and blood precipitate. 200 μL of plasma was then extracted with tert-butyl methyl ether (TBME) for analysis by HPLC. As shown by the HPLC results in Table 6A, there were differences in extraction for the two formulations (i.e. Taxol[®] and nanocrystals). For the same amount of paclitaxel spiked in the blood, the HPLC ratio (PTX/Internal STD) of Taxol[®] formulation is 2.86 times larger than that of the nanocrystal. To confirm that this difference is indeed due to extraction differences and not due to formulation itself, 10 μg of paclitaxel in plasma of both formulations were directly injected into HPLC, and similar HPLC ratio were obtained as shown in Table 6B (61.87 for Taxol[®] and 58.13 for nanocrystal). The nanocrystals extraction by tert-butyl methyl ether (TBME) was lower compared with that of Taxol[®]. To resolve the differences in extraction between the two formulations, 100 μL of acetonitrile was added to plasma samples to dissolve the nanocrystals prior to extraction by TBME (Figure 14). As shown in Table 6C, for the same amount of paclitaxel spiked in plasma, the HPLC ratios were similar for Taxol[®] and nanocrystal after the addition of acetonitrile prior to extraction by TBME.

2. Difference in Extraction Recovery of Plasma and Organs

In order to construct a paclitaxel in plasma standard curve, various amounts of paclitaxel were dissolved in plasma, and the internal standard (Butyl-4-hydroxybenzoate) was fixed in all plasma samples. After the addition of 100 μL of acetonitrile, the plasma samples containing paclitaxel and internal standard were extracted using tert-butyl methyl ether (T-BME) twice, and the organic phase was dried with a stream of nitrogen gas. The residue was then reconstituted with 100 μL of mobile phase, and 50 μL of the reconstituted samples were then injected into HPLC for analysis. The resulting paclitaxel plasma and organs standard curves were shown in figure 15, and the liver PTX standard curve was significantly differently from that of the other organs.

3. PTX Nanocrystal Biodistribution Study

The PTX nanocrystal biodistribution in mice plasma and organs 1 h post injection was displayed in figure 16. The plasma concentration of nanocrystal consists of only 12.63% of recovered dose, and the majority of the nanocrystal went to the liver (65.85%) due to rapid reticuloendothelial system (RES) uptake. It seems that F127 surfactant on the surface of nanocrystals could prevent aggregation, yet the surfactants were unable to protect the nanocrystals from RES uptake. The nanocrystals formed by F127 Pluronic formulation were of rod-shaped and of <150 nm in length. It was hoped that the small rod shaped nanocrystals could escape reticuloendothelial system (RES) uptake. Despite

this property, the biodistribution data shown indicated that the F127 nanocrystals formed were still largely taken up by the RES system and went into liver.

Discussion

Nanosuspensions are useful dosage forms for the formulation of water-insoluble drugs^{13,19}. Techniques such as high-pressure homogenization and wet milling are often used to produce nanosuspensions of small size suitable for pharmaceutical uses, these nanosuspensions are stabilized by surfactant such as Pluronic polymers for storage purposes to prevent aggregation^{20,21}. Studies have demonstrated that stable nanosuspensions of sparingly water-soluble drugs was comparable or improved over the response elicited by the conventional formulations; dosages could be increased without incidence of acute toxicity, abnormal weight loss, or organ pathology^{14,21}. Currently five products are on the market by the approval of FDA since the year 2000, all intended for oral delivery; all five products are based on top-down approaches such as media milling and high-pressure homogenization²². PTX/F127 nanocrystal is a nanosuspension formulation of PTX developed in our lab using stabilization of nanocrystals (SNC) method, and the objectives of this study were to further understand the structure and stability of the nanocrystals, as well as the biodistribution of the nanocrystals 1 h post injection *in vivo*.

The state of crystallinity of the nanocrystals was evaluated using X-ray powder diffraction. F127 is a semicrystalline polymer, with the crystalline phase consisting of PEO layers and amorphous layers formed by PPO and PEO²³. Nanocrystals, as well as PTX/F127 physical mixture, has the diffraction pattern consisting of both pure PTX and

F127 (figure 1), showing that the crystallinity of nanocrystals were unaltered by the preparation and lyophilization process. Because the PTX/F127 physical mixture and nanocrystals had very similar XRD patterns, TEM pictures were taken to observe compare the crystal growth morphology of physical mixture and nanocrystals (Figure 2). The pure PTX crystals were highly irregular in shape that aggregated with each other. While the PTX/F127 physical mixture had semblance of rod-shaped crystals, the crystals aggregated with each other into a mass because the F127 were unable to adequately stabilize the crystals. This shows that the co-solvation in chloroform and subsequent co-precipitation were important steps in preparing stable nanocrystals, without these steps, the crystals formed would collapse into a mass.

Hydrophobic interactions are negative entropic processes, therefore, the higher the temperature of the suspension, the more thermodynamically unfavorable the system becomes; in hydrophobic suspensions, the tendency of aggregation is enhanced at higher temperature¹⁵. Our nanocrystals stabilized by F127 surfactant increased in size upon 2 h incubation at 37 °C, becoming crystals of great length (figure 3). It has been reported that further increase in surfactant in nanosuspensions could afford thicker coating layer to the nanocrystals, thus providing better long-term stability^{17,24}. Therefore, in our study nanocrystals with increasing F127 surfactant were prepared (1/10, 1/20, 1/30 w/w PTX/F127). It was hoped that the increase in F127 could afford better stability against aggregation from 37 °C incubation. On the contrary however, nanocrystals with higher concentration of F127 surfactant increased even more in size after 2 h 37 °C incubation (Table 2). This trend was confirmed by manually measuring the nanocrystals in each TEM field-view (Table 3). The reason for this trend became clear from TEM (Figure 5),

instead of forming a thicker layer on the nanocrystals surface, micelles began to form in solution at higher concentration of F127. The CMC of Pluronic F127 at 25 °C is $7.19 \times 10^{-5} \text{ M}^{27}$. The concentration of F127 in nanocrystals prepared with 1/5 w/w of PTX/F127 is below the CMC of F127. However, for 1/10, 1/20, and 1/30 of PTX/F127, the concentration of surfactant goes beyond the CMC. After the attainment of the CMC, the micelles began to compete for surface adsorption so that the total adsorption at the interface begins to decrease as the micelles become more numerous²⁵. Another study on the adsorption of Pluronic polymers on the adsorption of DDS-glass by radiolabelling also confirmed this effect²⁶. Thus, the higher F127 surfactant concentration could actually mean less surfactant adsorption, which would further destabilize the nanocrystals during the 2 h 37 °C incubation, thus contributing to a larger size increase. Croy *et al.* studied the effects of Pluronic polymers on the aggregation state of poorly soluble nystatin. They found that nystatin could partition into pluronic micelles and the largest contributing factor to the solubilization of nystatin was the number and size of the micelles formed²⁷. However in our case PTX nanocrystals were stabilized by surface adsorption of F127 surfactant, and the formation of micelles would compete with F127 surface adsorption—thus destabilizing the nanocrystals.

The effects of dilution on size increase of nanocrystals prepared with varying amounts of F127 (1/5, 1/10, 1/20, 1/30 w/w) were studied. The nanocrystals were in a meta-stable state with free surfactant in solution and adsorbed surfactant for stabilization. By dilution it is hoped that the equilibrium would be shifted such that the adsorbed surfactant would leave the nanocrystals and go into the free form. If the surfactant does indeed leave, the crystal size increase would be detected. It was found that for

nanocrystals of 1/5 w/w PTX/F127, the dilution had no effect on size increase; however, nanocrystals prepared with higher amount of F127 (1/10, 1/20, 1/30 w/w) increased much in size upon dilution (Figure 7). The TEM of undiluted samples at the end of the experiment (Figure 8) revealed micelle formation in nanocrystals samples with higher concentration of surfactant (1/20, 1/30 w/w PTX/F127).

One study by Lin *et al.* using dynamic light scattering (DLS) and small-angle neutron scattering (SANS) found that below CMC PPO of Pluronic F127 preferred hydrophobic Carbon Black (CB) particle surface to water, but above CMC Pluronic F127 preferred to associate with each other and had decreased affinity to CB surface²⁸. Below CMC monolayer of F127 monomers bound to CB surface with high affinity, above CMC adsorbed layer thickness measured by DLS, as well as structure determined by SANS, suggested that the adsorbed layer was in the form of micelles²⁸. The observation that at higher bulk surfactant concentration, micelles, or monomer aggregates “hemi-micelles”, bound to hydrophobic surface with lower affinity is also confirmed by Amiji using radiolabelling methods²⁶. This is in line with our observation that at higher F127 concentration surface surfactants readily leave upon dilution, making the crystals increase in size. At higher F127 concentration where micellization occurs, F127 monomers on the surface aggregated with each other and consequently bound the surface with lower affinity.

It is known that the CMC of Pluronic F127 decreases strongly with increasing temperature, from 0.3 wt % at room temperature to 0.025 wt % at 37 °C¹⁶. At higher temperatures the surfactant adsorption is inhibited more than micellization, meaning that micellization will out-compete surface adsorption²⁹. At 37 °C nanocrystals of 1/5

PTX/F127 increased in size upon dilution concurrent with micelle formation (Figure 10), whereas at room temperature the same nanocrystals did not increase in sizes. This experiment thus showed again that in samples with micelle formation either because of high F127 concentration or induced by higher temperature, surface surfactant aggregated and bound the nanocrystals with lower affinity; the surfactant readily desorbed upon dilution, destabilizing nanocrystals and causing size increase.

The size increase of nanocrystals due to thermal induced aggregation at 37 °C incubation or Ostwald ripening at room temperature poses storage problems and could be undesirable. This negates important advantages of nanosuspensions, such as the increase in saturation solubility and increase in dissolution rate of compound³⁰. Nanosuspensions have shown increased antitumor efficacy by taking advantage of the Enhanced Permeability and Retention (EPR) effect during its prolonged retention time³¹. It would be difficult for large crystals to take advantage of the EPR effect. Therefore the “Incubation-Sonication” procedure was used to provide better stability of the nanocrystals. After the crystal size increased after the 2 h 37 °C incubation, sonication was used to break down the samples into smaller nanocrystals. After incubating at 37 °C for 2 hours, it was found that the “Incubation-Sonication” procedure (figure 11) effectively prevented the regrowth into longer crystals (figure 12). Closer examination by manual measuring in TEM revealed that the “Incubation-Sonication” procedure prevented the regrowth in length of the crystals; however, the growth in width of the crystals was statistically significant (Table 4). The growth in width was less favored by the nanocrystals. Therefore, the “Incubation-Sonication” procedure disturbed the growth pattern of the nanocrystals, thus providing better stability.

HPLC was used to analyze PTX in biodistribution studies, and it was found that there were extraction differences by tert-butyl methyl ether. The ratio of PTX to internal standard ratio was 2.86 times larger for Taxol[®] than for nanocrystals (Table 6A). As opposed to using excess co-solvents such as Cremophor EL to dissolve PTX, nanocrystal formulation is in a dense, solid state that has the property of higher mass per volume¹³. This could be the reason PTX extraction efficiency by TBME is lower for nanocrystals than for Taxol[®], and to resolve the difference, acetonitrile had to be added as a co-solvent to dissolve the nanocrystals prior to extraction (figure 14). PTX standard curves were constructed for plasma and organs, and it was found that the liver standard curve was significantly different from the others (Figure 15).

The biodistribution of nanocrystals 1 h post intravenous injection revealed that majority of nanocrystals (65.86%) were quickly taken up by the RES system and went to the liver (Figure 16). Several pharmacokinetic profiles have been reported for nanosuspensions after intravenous injection. If the particles dissolve in the blood readily, both the pharmacokinetics and tissue distribution will be equivalent to those for the solution formulations^{32,33}. However, there is evidence that our nanocrystals are slow-dissolving after injection into the blood stream. Previous studies have shown that slow dissolving nanocrystals were taken up by the phagocytic cells of the mononuclear phagocyte system (MPS), primarily the Kupffer cells in the liver, spleen, and lungs^{34,35}. The drug particles could dissolve in the reduced pH environment of the phagolysosomes³⁶ and slowly diffuse out of the MPS cells based on their lipophilic character¹³. This effect will result in a pharmacokinetic profile with significantly reduced C_{max} , but quite prolonged $t_{1/2}$, and this trend has been observed for nanosuspensions by

many studies^{20,37}. This can be very advantageous for certain drug classes, for which toxicity is mediated by peak plasma values, but for which efficacy is driven by AUC, as in the case of triazole antifungals³⁸.

Conclusion

In conclusion, the crystalline structure of PTX nanocrystals was unaltered from that of pure PTX based on X-ray Powder Diffraction analysis. The nanocrystal size increased after 2 h 37 °C incubation due to thermal induced aggregation, and more F127 surfactant further destabilized nanocrystals and led to a large size increase concurrent with micelle formation. Cytotoxicity on H460 cells indicate that increased F127 did not affect the cytotoxicity of the nanocrystals. PTX/F127 nanocrystals (1/5 w/w) had little size increase upon dilution, and nanocrystals of increasing F127 surfactant (1/20, 1/30 w/w) increased much in size upon dilution. At 37 °C where micellization is enhanced, even PTX/F127 nanocrystals (1/5 w/w) increased in size upon dilution. The “Incubation-Sonication” procedure effectively inhibited crystal growth after 37 °C by disturbing the preferred crystal growth pattern of PTX. The cytotoxicity and crystalline structure of nanocrystals were unaltered after “incubation-sonication” procedure. Finally, the biodistribution of nanocrystals revealed that majority of nanocrystals were quickly taken up by the reticuloendothelial system and went to the liver 1 h post injection.

Table 1. X-Ray Powder Diffraction Peaks and Corresponding d spacings for pure PTX, pure F127, nanocrystal, and PTX/F127 physical mixture.

2θ Angle	d spacing (Angstrom)	Pure PTX	Pure F127	Nanocrystal	Physical Mixture
9.8	9.02	Present (weak)		Present	Present
11	8.04	Present		Present (faint)	Present (weak)
12	7.38	Present		Present	Present
13.5	6.56	Present		Present	Present
19.5	4.55		Present	Present	Present
23.7	3.75		Present	Present	Present

Table 2. Nanocrystal size increase after 37 °C incubation for 2 hours. Nanocrystals prepared with various amounts of F127 were measured for their sizes before and after 37 °C incubation.

	Measured Size (nm) Before 37 °C Incubation	Measured Size (nm) After 37 °C Incubation
PTX/F127 (1/5 w/w)	176	258
PTX/F127 (1/10 w/w)	187	303
PTX/F127 (1/20 w/w)	158	359
PTX/F127 (1/30 w/w)	181	441

Table 3. Size of nanocrystals prepared with various amounts of F127 determined by manual measuring in TEM. At least 20 crystals were measured for each sample. **For the length of nanocrystal, $P < 0.05$ when compared to either PTX (1/10), (1/20), or (1/30).

	Measured Size (nm) Before 37 °C incubation	Measured Size (nm) After 37 °C incubation
PTX/F127 (1/5 w/w)	37 × 160** (±7 × ±47)	53 × 660** (±18 × ±318)
PTX/F127 (1/10 w/w)	39 × 297 (±10 × ±113)	57 × 971 (±14 × ±324)
PTX/F127 (1/20 w/w)	45 × 322 (±11 × ±82)	47 × 1273 (±10 × ±652)
PTX/F127 (1/30 w/w)	37 × 344 (±10 × ±149)	-----

Table 4. The size of nanocrystals prepared by manual measurements in TEM. Samples are PTX/F127 nanocrystals before 37 °C incubation (Sample A), nanocrystals after 37 °C incubation then sonication (Sample B), nanocrystals after 37 °C incubation, sonication, then 37 °C incubation again (Sample C). The increases in length of sample C was not statistically significant compared to A or B. *For the width of nanocrystals, $p < 0.05$ compared to either Sample A and B.

	Measured Size (nm)
Sample A PTX/F127 Before 37 °C (1/5 w/w)	37 × 160 (±7 × ±47)
Sample B PTX/F127 37 °C – Sonication (1/5 w/w)	63 × 177 (±7 × ±46)
Sample C PTX/F127 37 C – Sonication – 37 °C (1/5 w/w)	73* × 185 (±12 × ±68)

Table 5. X-ray Powder Diffraction Analysis of nanocrystals after the “Sonication-Incubation” procedure. The crystalline structure were unaltered for (1) nanocrystals after 37 °C incubation and (2) nanocrystals after 37 °C incubation, then sonication, then incubated at 37 °C for 2 h again.

2θ Angle	d spacing (Angstrom)	Pure PTX	Pure F127	Nanocrystal 37 °C Incubation	Nanocrystal 37 °C Incubation Sonication 37 °C Incubation
9.8	9.02	Present (weak)		Present	Present
11	8.04	Present		Present	Present
12	7.38	Present		Present	Present
13.5	6.56	Present		Present	Present
19.5	4.55		Present	Present	Present
23.7	3.75		Present	Present	Present

Table 6. (A) HPLC plasma results of 600 μ L of blood spiked with 50 μ g of paclitaxel extracted with TBME **without** the addition of acetonitrile prior to extraction (B) HPLC results of 10 μ g of paclitaxel by direct injection (C) HPLC plasma results of 600 μ L of blood spiked with 10 μ g of paclitaxel extracted with TBME **with** the addition of acetonitrile prior to extraction.

A)

Name	Retention Time	Area	Ratio
Plasma Taxol [®]	22.4	11956375	(PTX/Int)
Internal Standard	12.8	47329.08	252.6
Name	Retention Time	Area	Ratio
Plasma Nanocrystal	22.5	4108067	(PTX/Int)
Internal Standard	12.9	46524.07	88.3

B)

Name	Retention Time	Area	Ratio
Internal Standard	12.1	54806.8	(PTX/Int)
Taxol [®] (10 μ g) Direct Injection	18.5	3390698	61.9
Name	Retention Time	Area	Ratio
Internal Standard	12.1	55726.55	(PTX/Int)
Nanocrystal (10 μ g) Direct Injection	18.5	3239422	58.1

C)

Name	Retention Time	Area	Ratio
Internal Standard	12.2	49270.75	(PTX/Int)
Plasma Taxol [®] (with Acetonitrile)	18.6	1478042	30.0
Name	Retention Time	Area	Ratio
Internal Standard	12.3	42690.28	(PTX/Int)
Plasma Nanocrystal (with Acetonitrile)	18.8	1175104	27.5

Figure 1. X-Ray Powder Diffraction Peaks for A) pure paclitaxel B) pure F127 C) nanocrystals and physical mixture of PTX and F127.

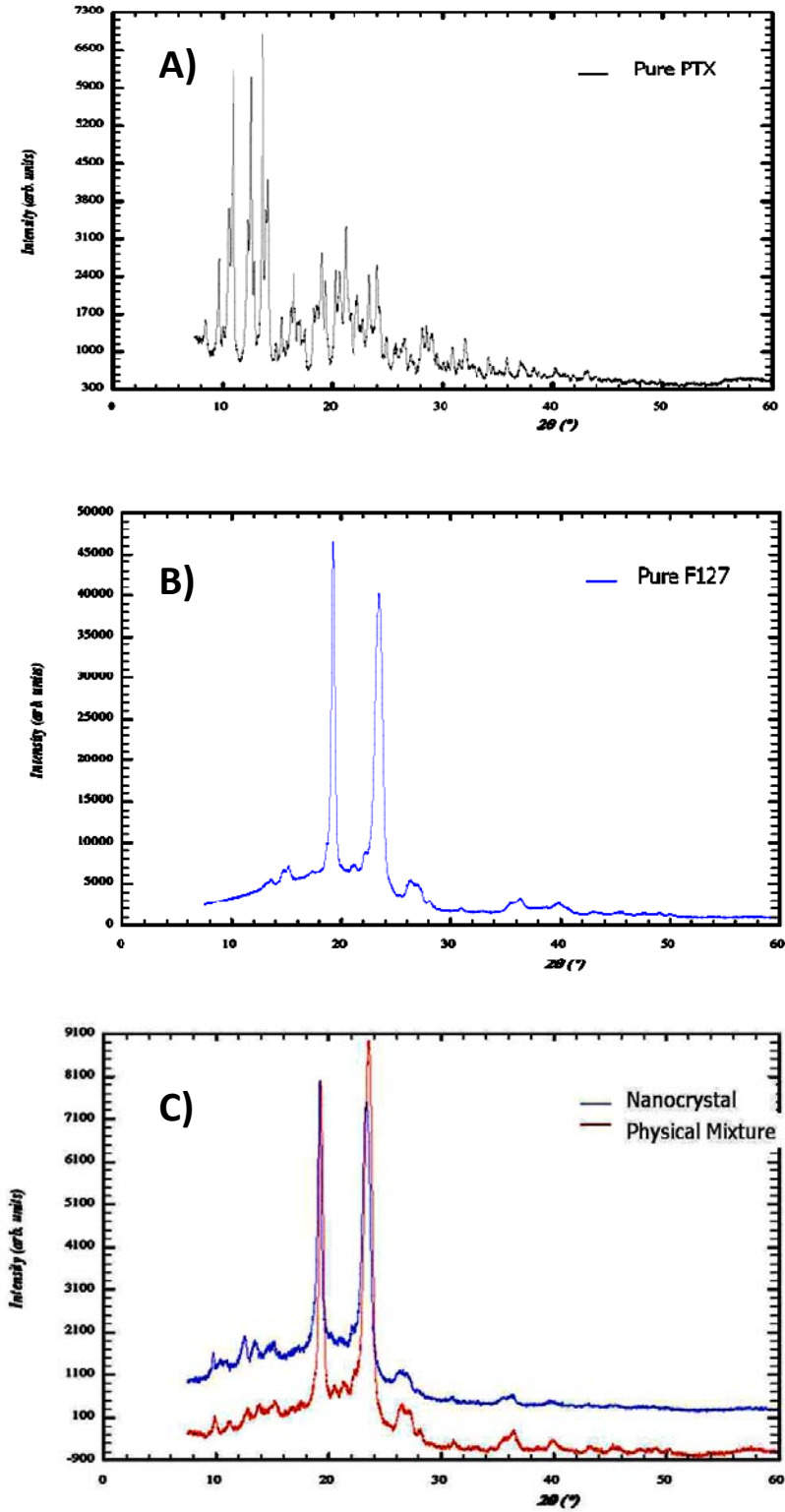


Figure 2. TEM pictures of A) PTX/F127 nanocrystals (1/5 w/w) B) PTX crystal without addition of F127 surfactant. C) Physical mixture of PTX and F127 surfactant.

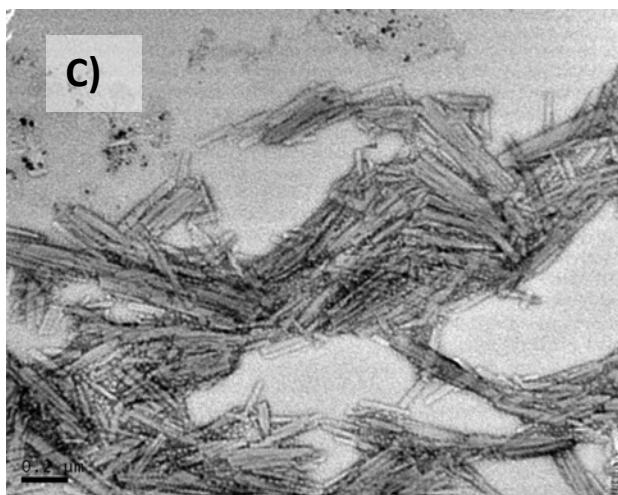
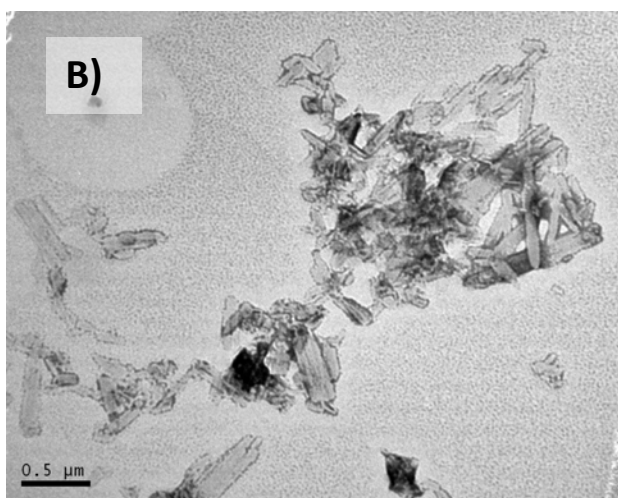
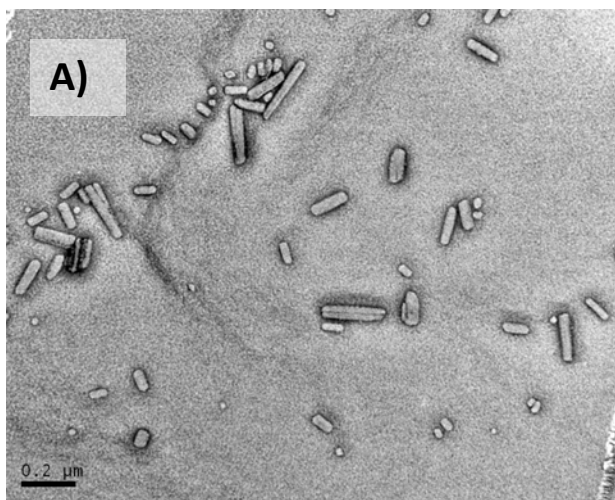


Figure 3. TEM pictures of nanocrystals for thermal stability studies. A) Nanocrystals before 37 °C incubation. Measured size using ZetaSizer 176 nm B) Longer crystals formed by incubation at 37 °C for 2 hours. Measured size using ZetaSizer 258 nm.

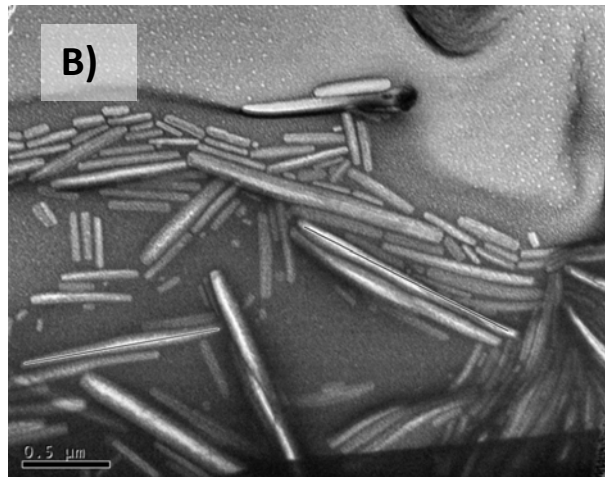
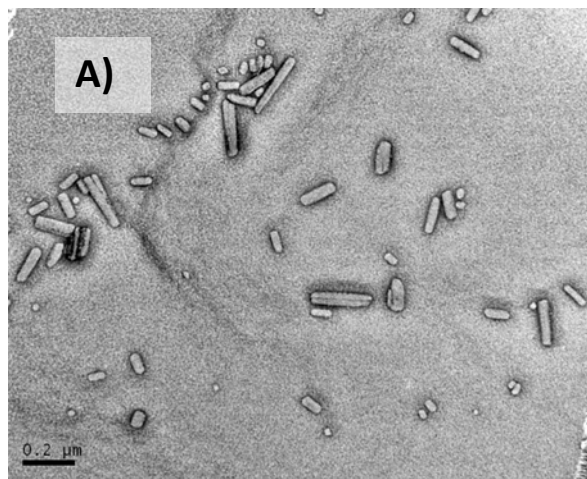


Figure 4. Effects of Increasing F127 Concentrations on Nanocrystal Cytotoxicity. Nanocrystals of 1/10, 1/20, 1/30 w/w PTX/F127 were prepared and applied to H460 cells. F127 of various concentrations without PTX were also tested. Each data represents the mean \pm standard deviation ($n = 6$).

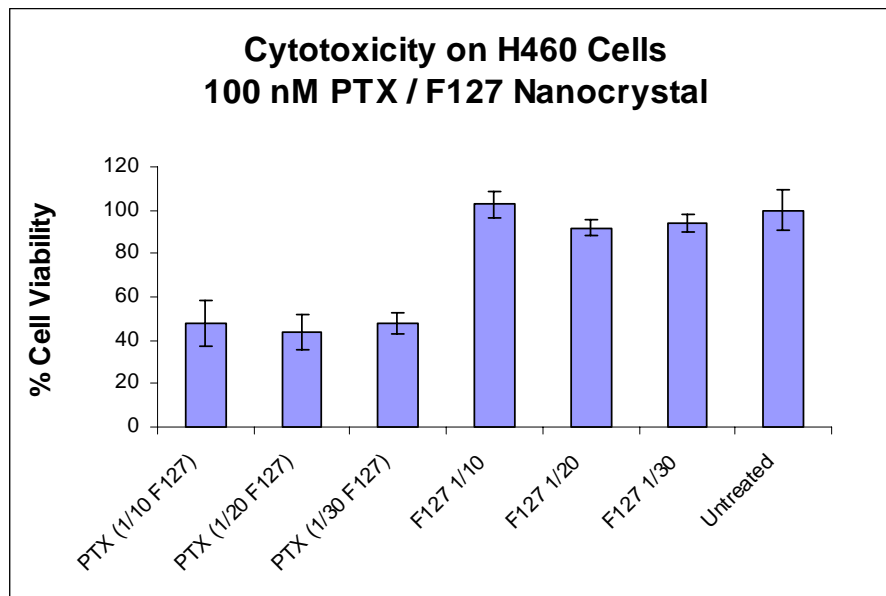


Figure 5. TEM of nanocrystals of A) PTX/F127 (1/10 w/w) and B) PTX/F127 (1/20 w/w). The white spherical structures in the background are micelles formed at high concentration of F127.

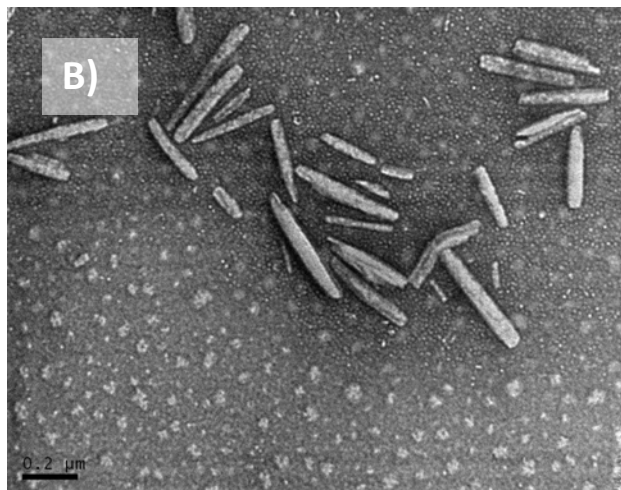
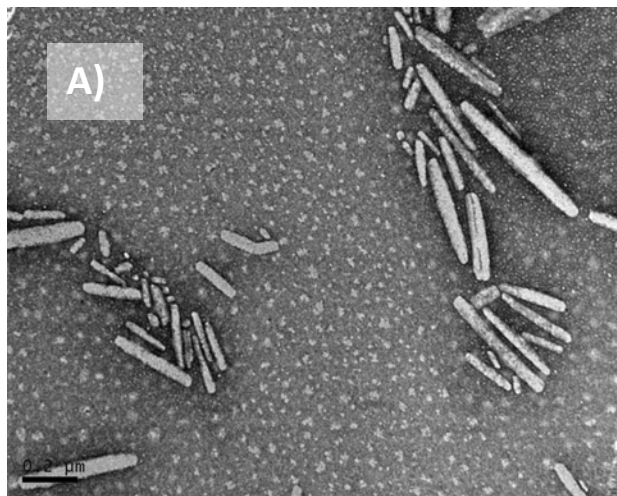


Figure 6. Illustration of nanocrystal stabilized by F127 at either low (1/5 w/w PTX/F127) or high concentration (1/20, 1/30 w/w PTX/F127). For nanocrystals prepared with low concentration of F127, monomers bound with high affinity. As more F127 was added, there was micelles formation in solution and formation of surfactant aggregates (hemi-micelles) on nanocrystal surface. Micelles could also compete for surface adsorbed F127 surfactants.

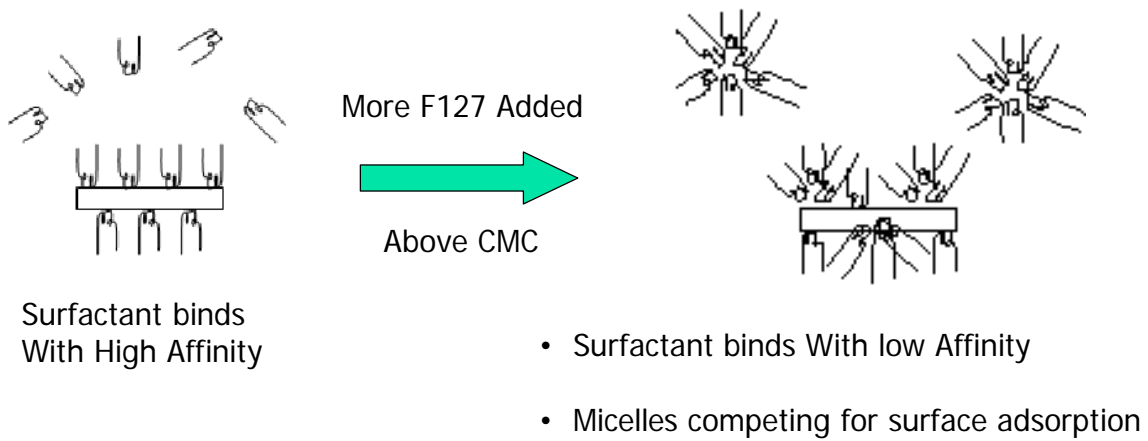


Figure 7. Nanocrystal Size increase upon dilution at room temperature. A) Nanocrystals (1:5 w/w PTX/F127). B) Nanocrystals (1:10 w/w PTX/F127). C) Nanocrystals (1:20 w/w PTX/F127). D) Nanocrystals (1:30 w/w PTX/F127). Data represents mean value for at least 20 readings for each sample.

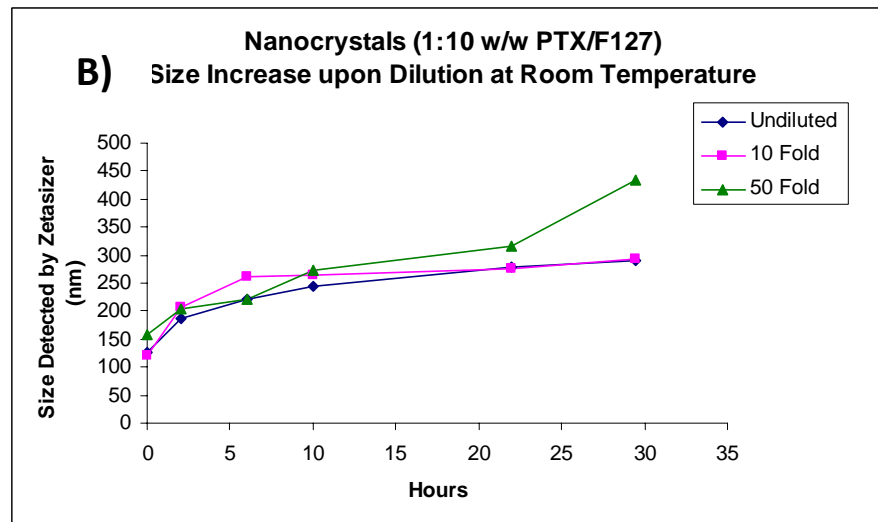
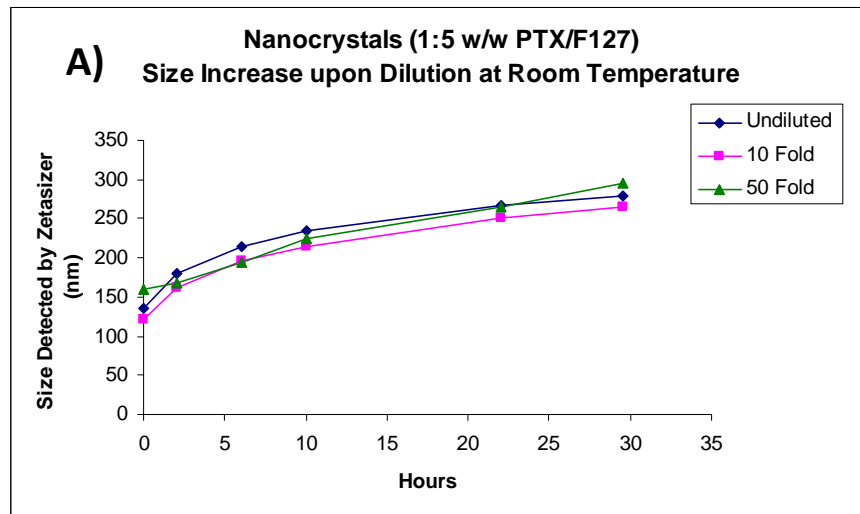


Figure 7. Nanocrystal Size increase upon dilution. A) Nanocrystals (1:5 w/w PTX/F127). B) Nanocrystals (1:10 w/w PTX/F127). C) Nanocrystals (1:20 w/w PTX/F127). D) Nanocrystals (1:30 w/w PTX/F127). Data represents mean value for at least 20 readings for each sample.

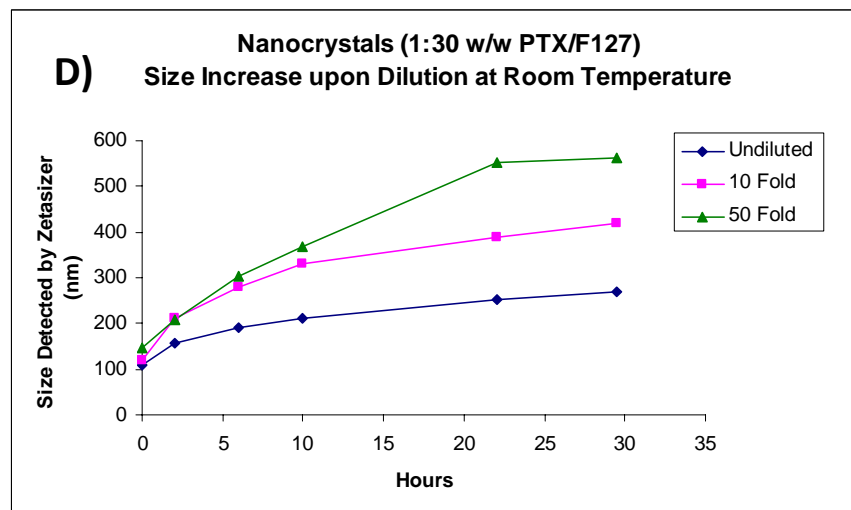
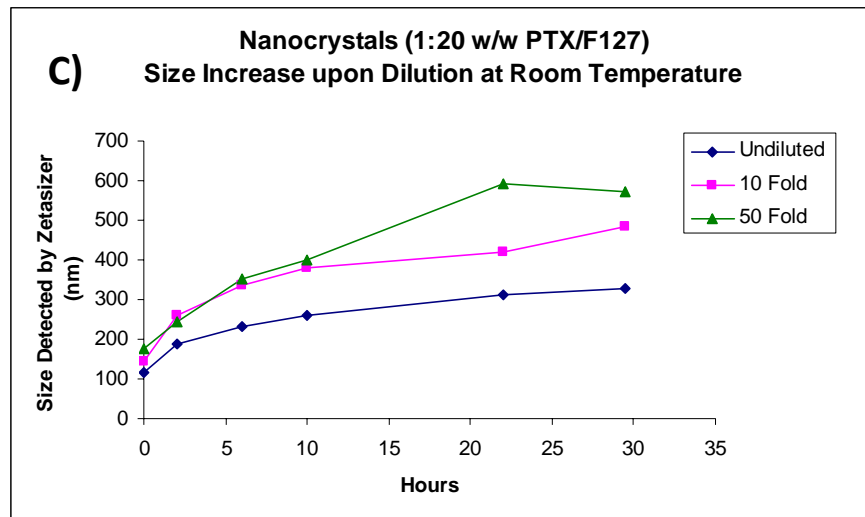


Figure 8. TEM of undiluted samples at the end of dilution-size experiment at room temperature. Notice the formation of micelles in samples with higher F127 concentrations. A) PTX/F127 (1/5 w/w) B) PTX/F127 (1/10 w/w) C) PTX/F127 (1/20 w/w) D) PTX/F127 (1/30 w/w).

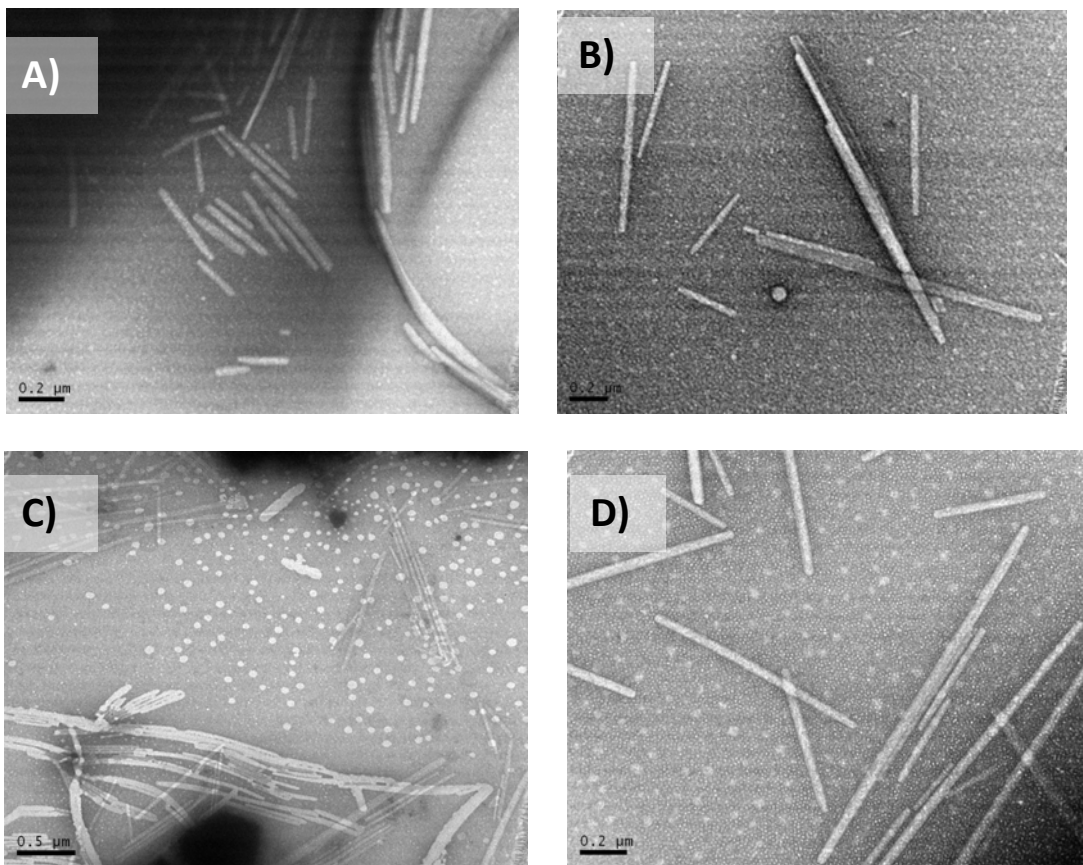


Figure 9. Size increase of nanocrystals with high F127 concentration upon dilution. In nanocrystals prepared with high concentration of F127, there was micelle formation in solution and formation of hemi-micelles on nanocrystal surface. These low affinity hemi-micelles readily left the surface upon dilution, leading to crystal growth and aggregation.

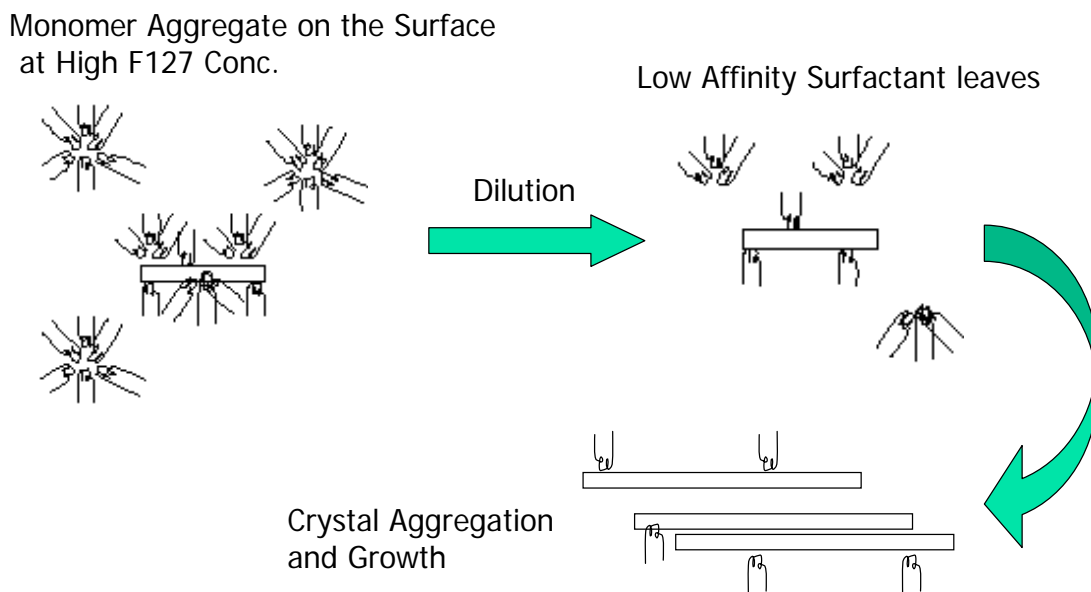


Figure 10. Nanocrystal (1:5 w/w PTX/F127) size increase upon dilution at 37 °C. Data represents mean value for at least 20 readings for each sample.

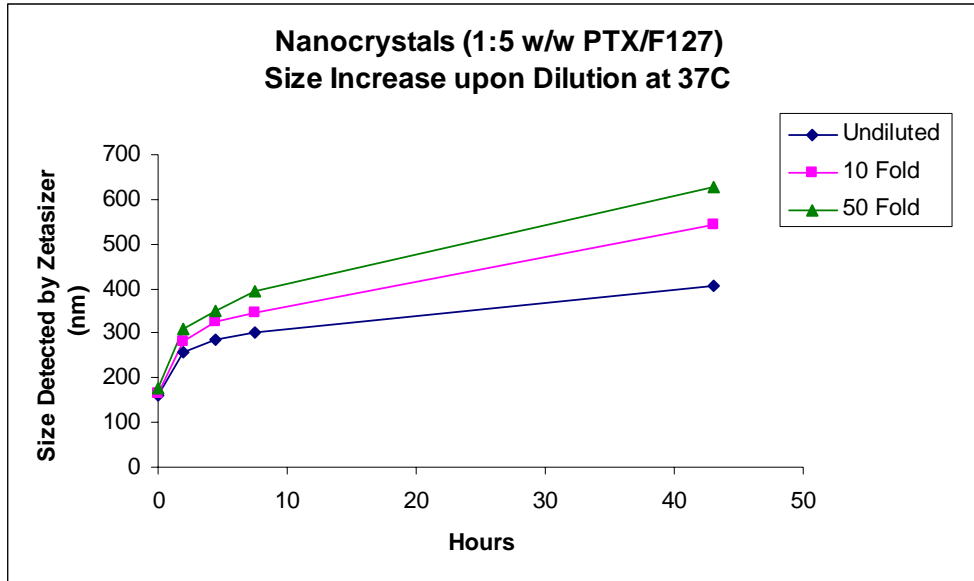
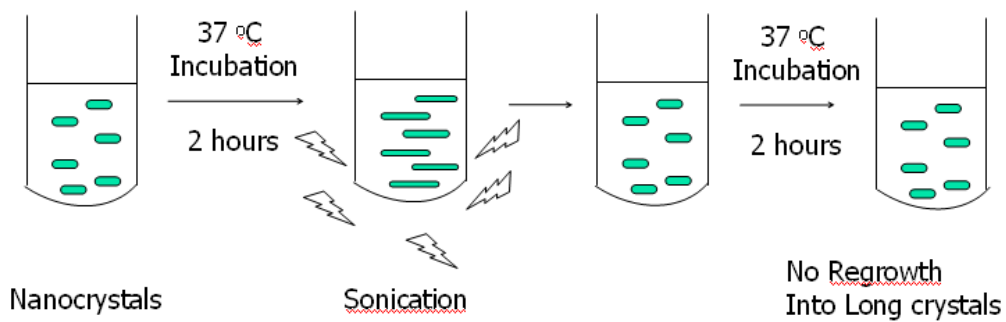


Figure 11. Re-nanonization by the “Incubation-Sonication” procedure. After 37 °C incubation long crystals were formed due to thermal induced aggregation. Sonication was used to break down long crystals into small nanocrystals again. After 37 °C incubation for the second time, no regrowth in length was observed for these small nanocrystals.



Courtesy of Yang Liu

Figure 12. Nanocrystal TEM pictures after Incubation-Sonication procedure. A) Break down of long crystals into nanocrystals by sonication for 15 min after 2 h 37 °C incubation. Measured size by ZetaSizer 139 nm. B) No observed regrowth into long crystals by incubating again at 37 °C incubation for 2 hours. Measured Size by ZetaSizer 163 nm.

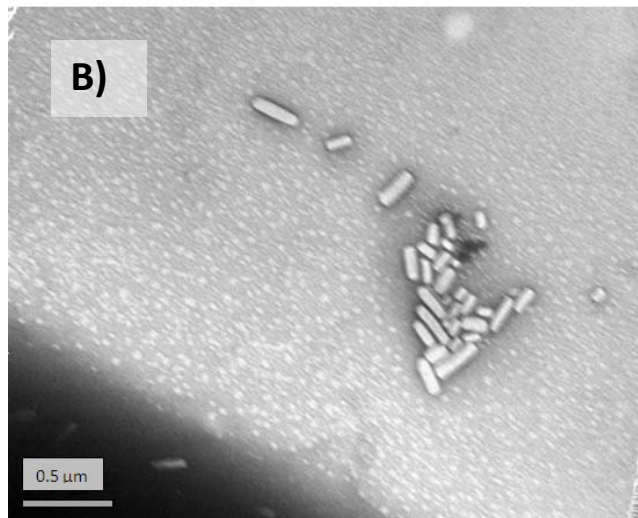
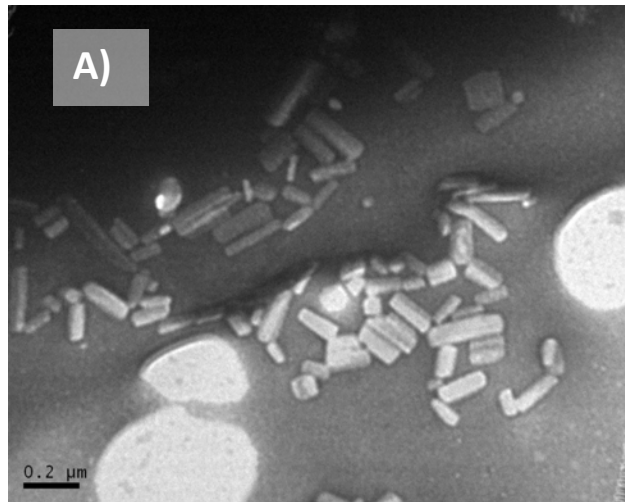


Figure 13. Cytotoxicity of Nanocrystals after “Incubation-Sonication” procedure 1) before 2 hr 37 °C incubation, 2) after 2 hr 37 °C incubation, 3) after 2 hr 37 °C incubation then sonication, 4) after 2 hr 37 °C incubation then sonication then 2 hr 37 °C incubation again. Each data represents the mean \pm standard deviation ($n = 8$).

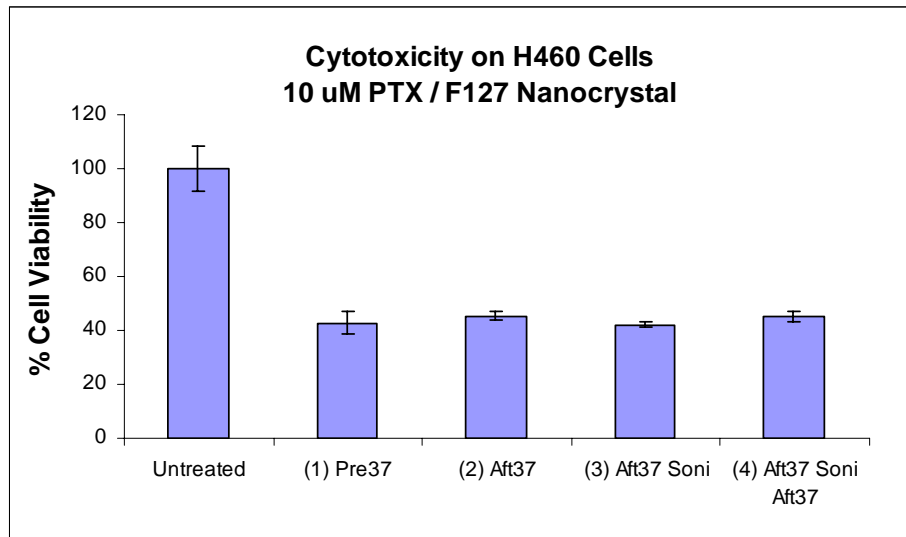


Figure 14. Extraction procedures of PTX with addition of acetonitrile. Acetonitrile was added to dissolve the nanocrystal structure prior to the extraction with tert-butyl methyl ether (TBME)

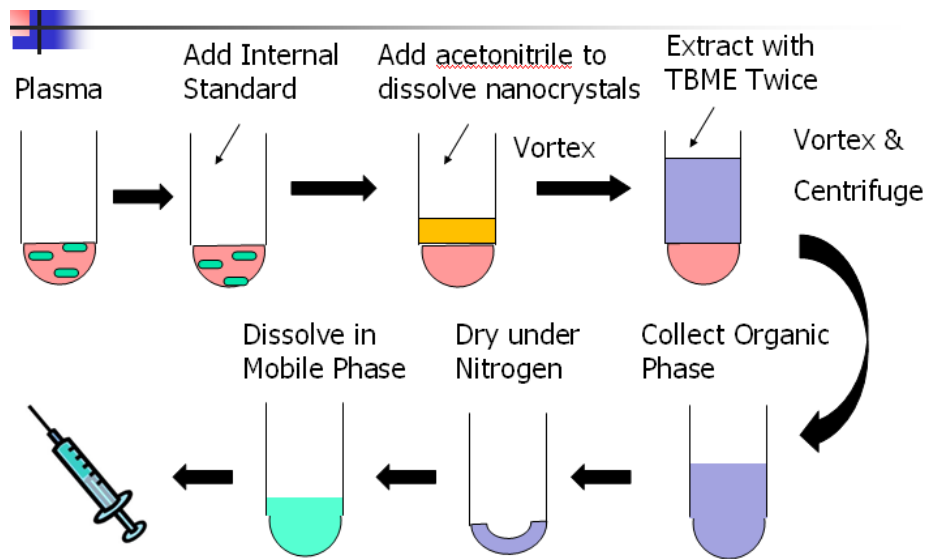
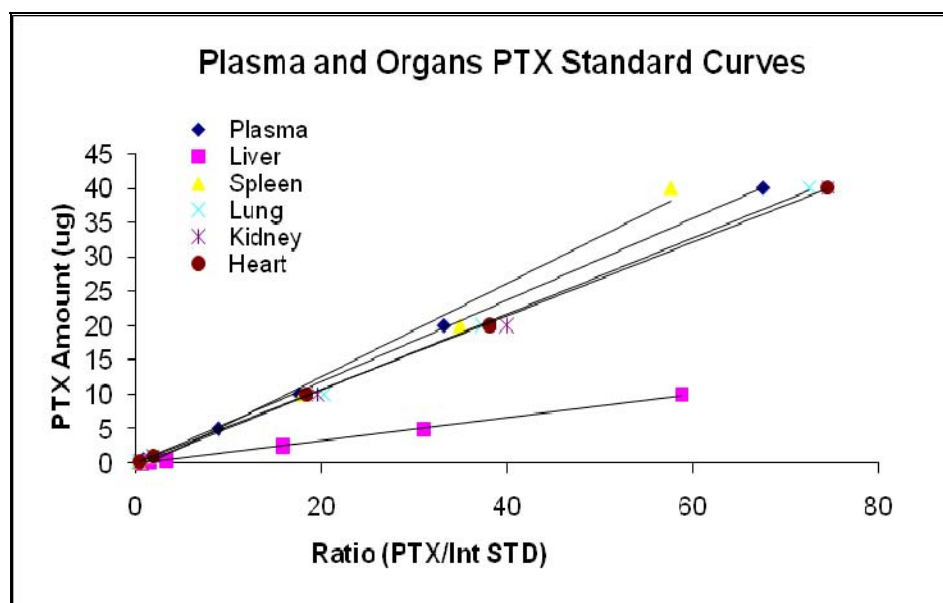
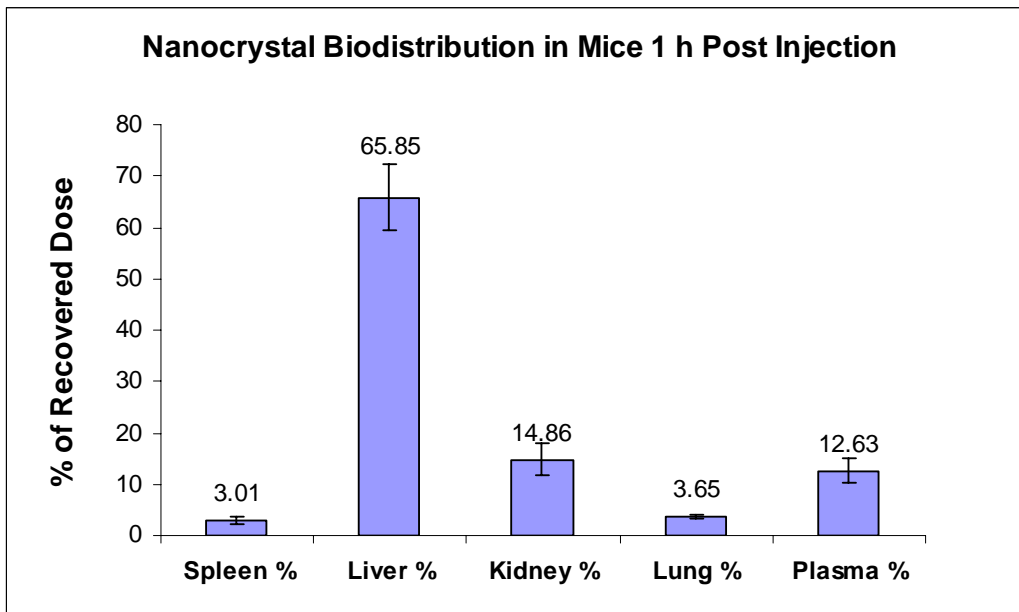


Figure 15. Plasma and Organs PTX Extraction Standard Curves. The best-fit equations to the data points are shown below the graph with y representing PTX amounts (μg) and x representing Ratio (PTX/Internal standard).



Plasma	$y=0.594x-0.1081$	Lung	$y=0.5516x-0.3605$
Liver	$y=0.1695x-0.088$	Kidney	$y=0.5335x-0.3405$
Spleen	$y=0.677x-0.9986$	Heart	$y=0.5354x-0.0348$

Figure 16. Nanocrystals biodistribution in mice plasma and organs 1 h post injection. Each data represents the mean \pm standard deviation ($n = 5$).



References

1. Singla AK, Garg A, Aggarwal D 2002. Paclitaxel and its formulations. *Int J Pharm* 235(1-2):179-192.
2. Kim SC, Kim DW, Shim YH, Bang JS, Oh HS, Wan Kim S, Seo MH 2001. In vivo evaluation of polymeric micellar paclitaxel formulation: toxicity and efficacy. *J Control Release* 72(1-3):191-202.
3. Rowinsky EK, Donehower RC 1995. Paclitaxel (taxol). *N Engl J Med* 332(15):1004-1014.
4. Cheon Lee S, Kim C, Chan Kwon I, Chung H, Young Jeong S 2003. Polymeric micelles of poly(2-ethyl-2-oxazoline)-block-poly(epsilon-caprolactone) copolymer as a carrier for paclitaxel. *J Control Release* 89(3):437-446.
5. Lasser EC, Walters A, Reuter SR, Lang J 1971. Histamine release by contrast media. *Radiology* 100(3):683-686.
6. Na GC, Stevens HJ, Jr., Yuan BO, Rajagopalan N 1999. Physical stability of ethyl diatrizoate nanocrystalline suspension in steam sterilization. *Pharm Res* 16(4):569-574.
7. Bohm BH, Muller RH 1999. Lab-scale production unit design for nanosuspensions of sparingly soluble cytotoxic drugs. *Pharm Sci Technolo Today* 2(8):336-339.
8. Hintz RJ, KC. 1989. The effect of particle size distribution on dissolution rate and oral absorption. *International Journal of Pharmaceutics* 51:9-17.
9. Liversidge GG, Cundy KC 1995. Particle-Size Reduction for Improvement of Oral Bioavailability of Hydrophobic Drugs .1. Absolute Oral Bioavailability of Nanocrystalline Danazol in Beagle Dogs. *International Journal of Pharmaceutics* 125(1):91-97.
10. Peters K, Leitzke S, Diederichs JE, Borner K, Hahn H, Muller RH, Ehlers S 2000. Preparation of a clofazimine nanosuspension for intravenous use and evaluation of its therapeutic efficacy in murine *Mycobacterium avium* infection. *Journal of Antimicrobial Chemotherapy* 45(1):77-83.
11. Pignatello R, Bucolo C, Ferrara P, Maltese A, Puleo A, Puglisi G 2002. Eudragit RS100 (R) nanosuspensions for the ophthalmic controlled delivery of ibuprofen. *European Journal of Pharmaceutical Sciences* 16(1-2):53-61.
12. Jacobs C, Muller RH 2002. Production and characterization of a budesonide nanosuspension for pulmonary administration. *Pharmaceutical Research* 19(2):189-194.

13. Rabinow BE 2004. Nanosuspensions in drug delivery. *Nature Reviews Drug Discovery* 3(9):785-796.
14. Liu FP, JY. Zhang, Y. Conwell, C. Bathula, SR. Huang, L. 2009. Targeted Cancer Therapy with Novel High Drug-Loading Nanocrystals. In submission.
15. Lu SP, RJ. Forssberg, KSE. 2005. *Interfacial Separation of Particles*. ed., Amsterdam: Elsevier. p 427.
16. Linse P, Malmsten M 1992. Temperature-Dependent Micellization in Aqueous Block Copolymer Solutions. *Macromolecules* 25(20):5434-5439.
17. Van Eerdenbrugh B, Froyen L, Van Humbeeck J, Martens JA, Augustijns P, Van den Mooter G 2008. Drying of crystalline drug nanosuspensions-the importance of surface hydrophobicity on dissolution behavior upon redispersion. *Eur J Pharm Sci* 35(1-2):127-135.
18. Arunkumar ND, M. Rani, C. 2009. Nanosuspension technology and its applications in drug delivery. *Asian Journal of Pharmaceutics* 3:168-173.
19. Muller RH, Peters K 1998. Nanosuspensions for the formulation of poorly soluble drugs - I. Preparation by a size-reduction technique. *International Journal of Pharmaceutics* 160(2):229-237.
20. Ganta S, Paxton JW, Baguley BC, Garg S 2009. Formulation and pharmacokinetic evaluation of an asulacrine nanocrystalline suspension for intravenous delivery. *International Journal of Pharmaceutics* 367(1-2):179-186.
21. Merisko-Liversidge E, Sarpotdar P, Bruno J, Hajj S, Wei L, Peltier N, Rake J, Shaw JM, Pugh S, Polin L, Jones J, Corbett T, Cooper E, Liversidge GG 1996. Formulation and antitumor activity evaluation of nanocrystalline suspensions of poorly soluble anticancer drugs. *Pharm Res* 13(2):272-278.
22. Van Eerdenbrugh B, Van den Mooter G, Augustijns P 2008. Top-down production of drug nanocrystals: Nanosuspension stabilization, miniaturization and transformation into solid products. *International Journal of Pharmaceutics* 364(1):64-75.
23. Shatalova OV, Krivandin AV, Aksenova NA, Solov'eva AB 2008. Structure of pluronic F-127 and its tetraphenylporphyrin complexes: X-ray diffraction study. *Polymer Science Series A* 50(4):417-421.
24. Jacobs C, Kayser O, Muller RH 2000. Nanosuspensions as a new approach for the formulation for the poorly soluble drug tarazepide. *International Journal of Pharmaceutics* 196(2):161-164.

25. Chatterjee P, Gupta BS. . 2002. Absorbent Technology. ed., Amsterdam: Elsevier. p 162.
26. Amiji MM, Park K 1994. Analysis on the Surface-Adsorption of PEO-PPO-PEO Triblock Copolymers by Radiolabeling and Fluorescence Techniques. *Journal of Applied Polymer Science* 52(4):539-544.
27. Croy SR, Kwon GS 2004. The effects of Pluronic block copolymers on the aggregation state of nystatin. *Journal of Controlled Release* 95(2):161-171.
28. Lin YN, Alexandridis P 2002. Temperature-dependent adsorption of pluronic F127 block copolymers onto carbon black particles dispersed in aqueous media. *Journal of Physical Chemistry B* 106(42):10834-10844.
29. Rosen MJ. 2004. Surfactants and interfacial phenomena. 3rd ed., Hoboken, N.J.: Wiley-Interscience. p xiii, 444 p.
30. Kocbek P, Baumgartner S, Kristl J 2006. Preparation and evaluation of nanosuspensions for enhancing the dissolution of poorly soluble drugs. *International Journal of Pharmaceutics* 312(1-2):179-186.
31. Lou HY, Zhang XM, Gao L, Feng FF, Wang JY, Wei XB, Yu ZQ, Zhang DR, Zhang Q 2009. In vitro and in vivo antitumor activity of oridonin nanosuspension. *International Journal of Pharmaceutics* 379(1):181-186.
32. Clement Mea 1992. Tissue distribution and plasma clearance of a novel microcrystal-encapsulated flurbiprofen formulation. *The Pharmacologist* 34:204.
33. Gassmann P, List M, Schweitzer A, Sucker H 1994. Hydrosols - Alternatives for the Parenteral Application of Poorly Water-Soluble Drugs. *European Journal of Pharmaceutics and Biopharmaceutics* 40(2):64-72.
34. Gao L, Zhang DR, Chen MH, Duan CX, Dai WT, Jia LJ, Zhao WF 2008. Studies on pharmacokinetics and tissue distribution of oridonin nanosuspensions. *International Journal of Pharmaceutics* 355(1-2):321-327.
35. Moghimi SM, Hunter AC, Murray JC 2001. Long-circulating and target-specific nanoparticles: Theory to practice. *Pharmacological Reviews* 53(2):283-318.
36. Mukherjee S, Ghosh RN, Maxfield FR 1997. Endocytosis. *Physiological Reviews* 77(3):759-803.
37. Connelly Jea 2001. Pharmacokinetics of a 14 day course of itraconazole nanocrystals given intravenously to allogeneic haematopoietic stem cell transplant (HCST) recipient. 41st Intersci Conf Antimicrob Agents Chemother A32.

38. Andes D 2003. In vivo pharmacodynamics of antifungal drugs in treatment of candidiasis. *Antimicrobial Agents and Chemotherapy* 47(4):1179-1186.